Fatigue Crack Growth and Retardation in the Welded HAZ of 4140 Steel

Although samples represented four different conditions they displayed a similar resistance to fatigue crack growth

BY J. K. LIM AND R. I. STEPHENS

ABSTRACT. Room-temperature fatigue crack growth behavior was obtained for 4140 base metal, 4140 postweld heat treated base metal (PWHT), as-welded HAZ, and PWHT HAZ material under $R \approx 0$ and 0.5 constant amplitude loading and single tensile overloads with an OLR of 2.5. Two-pass automatic submerged arc welding with AWS EM2 electrode was used. Postweld heat treatment was performed at 650°C (1202°F) for 1 h. Constant amplitude fatigue crack growth behavior was very similar for all four material conditions in the log-log linear Paris region. All material conditions responded favorably to the single tensile overloads with fatigue crack growth retardation ranging from 2×10^5 to 6×10^5 cycles, which corresponded to life increases of 150 to 600%. Furthermore, scanning electron microscope (SEM) analysis indicated many similarities on the fatigue fracture surfaces with predominant ductile quasi-striation morphology.

Introduction

Unstable brittle fracture of welded structures and components is an active international problem (Ref. 1). Brittle fracture of welded structures often starts from the heat-affected zone (HAZ) (Refs. 2–4). A weldment, especially the HAZ, is a very complicated and variable structure formed from different thermal and environmental conditions (Refs. 5, 6). This complexity involves inherent mechanical behavior such as strength, ductility, hardness and fracture toughness. In addition, three-dimensional residual stress/strain can result in significant decrease of fracture toughness in the HAZ (Refs. 7–9). Therefore, in welding low-alloy steels such as 4140, postweld heat treatment (PWHT) is a common practice for removing undesirable residual tensile stresses along with reheat for repairing (Refs. 10, 11). Very high PWHT, over 600°C (1112°F), of these steels, however, can cause a coarse-grained region near the fusion line of the HAZ resulting not only in embrittlement, but also in stress relief cracking (Refs. 12, 13). Lim (Ref. 14), using CTOD fracture toughness and fracture surface observations, showed that the degree of PWHT embrittlement is dependent upon heating rate, holding time, applied stress and grain size of the weld HAZ microstructure.

Most welded structures and components are subjected to variable amplitude loading. Initial cracks can then grow under cyclic load to fracture. Both high- and low-amplitude cycles, along with constant-amplitude cycles, can occur in welded structures and components. Hence, sequence or interaction effects are of importance in calculating fatigue crack growth life of weldments. High-tensile overloads followed by low-amplitude loading can involve appreciable retardation of fatigue crack growth. This retardation has been attributed to crack tip blunting, residual compressive stresses in front of the crack tip and to crack closure (Ref. 15). In order to better calculate fatigue crack growth life in weldments, this retardation influence must be known quantitatively. Very little fatigue crack growth retardation information exists for weldments. Therefore, the purpose of this research is to contribute to the needed information for safe design and service life of weldments, particularly the HAZ, subjected to both constant-amplitude and single tensile overloads. This contribution is achieved using 4140 steel evaluated by fatigue testing, scanning electron microscopy (SEM) and recrystallization zones around the fatigue crack. Specifically, single tensile overload influences on constant-amplitude loading, with the stress ratio R approximately zero and 0.5, were obtained under four material conditions as follows: 1) base metal, 2) heat treated (same as PWHT) base metal, 3) as-welded HAZ, and 4) PWHT HAZ.

KEY WORDS

Weldments
Fatigue Crack Growth
Residual Stress
Crack Closure
Crack Retardation
Plastic Zone
Fractography
HAZ
PWHT
4140 Steel

Test Materials

The base metal used in this research was 4140 vacuum-degassed steel. Chemical composition and monotonic tensile properties in the rolled direction are given in Tables 1 and 2, respectively. Steel plate with 25-mm (1-in.) thickness was cut into 150 × 610-mm (6 × 24-in.) sections and a U-shaped groove, 610 mm long, was cut perpendicular to the rolled direction. The U groove was then welded using an automatic submerged arc welding machine with two passes. The electrode used was AWS EM2 and the flux was AWS F9A6. The welding conditions are given in Table 3. Figure 1 shows the weld section configuration along with the position of compact type, C(T), specimens used for all fatigue tests. A typical macroetched weld bead with the 25-mm-thick cross-section is shown in Fig. 2. The deposit metal appears as typical dendrite structure and the weld HAZ is located vertically for satisfactory extraction of C(T) specimens. Chemical compositions of the electrode and deposit metal are given in Table 1, and monotonic tensile properties in the long direction of the weld deposit (as-welded condition), obtained from tensile specimens, are given in Table 2.

Compact type, C(T), specimens with

J. K. LIM is Chairman and Associate Professor, Mechanical Engineering Department, Chonbuk National University, Chonju, Republic of Korea. R. I. STEPHENS is Professor, Mechanical Engineering Department, The University of Iowa, Iowa City, Iowa.

height/width (H/W) = 0.6 and final thickness equal to 8.2 mm (0.32 in.) were used for all fatigue tests. All dimensions were in accordance with ASTM Standard E647 (Ref. 16). The significant dimensions are given in Fig. 3. The chevron notched specimens were machined so that the fatigue crack would grow through the weld HAZ fusion line parallel to the weld direction and perpendicular to the rolled direction. Prior to heat treatment, the C(T) specimens were machined to overall planar dimensions with a thickness of 8.5 mm (0.33 in.). After heat treatment, all specimens were ground to final dimensions to remove surface decarburization. Heat treatment was performed on both welded and base metal C(T) specimens as follows: heating rate = 220°C/h (396°F/h), heating temperature = 650°C (1202°F), hold time = 1 h and cooling rate = 110°C/h (198°F/h).

The microstructures of the 4140 base metal, before and after heat treatment, are shown in Fig. 4, and the microstructures of the welded HAZ, before and after PWHT, are shown in Fig. 5. The microstructures of the 4140 base metal are essentially identical before and after heat treatment and consist of typical martensite structure with finely dispersed alloy carbides. The weld HAZ through the fusion line has a coarse-grained microstructure that is very similar before and after PWHT. According to Kameda, *et al.* (Ref. 7), and Dolby (Ref. 17), the prior austenite grain size near the fusion line affects the fracture toughness. A larger grain size produces a lower fracture toughness.

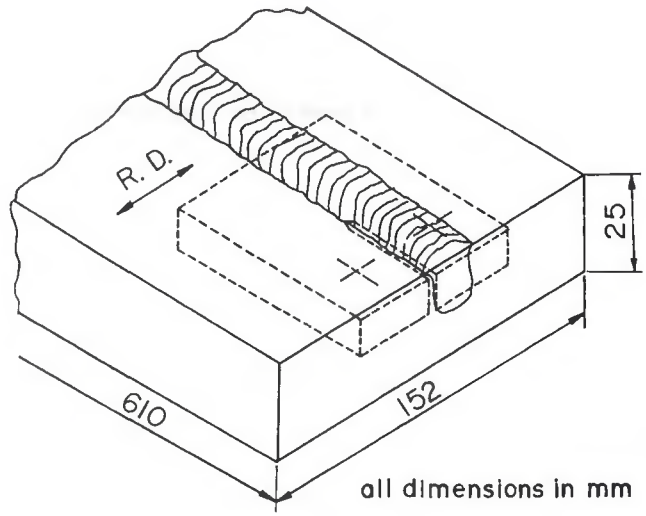

Fig. 1—Weld plate configuration and position of C(T) specimens.

Experimental Procedures

Fatigue Tests

All fatigue tests were performed at room temperature using an 89-kN closed-loop electrohydraulic test system in load control. The C(T) specimens were mounted in a pin/hole gripping system. Prior to specimen mounting, the tip of the chevron notch was sharpened using a razor blade for quicker crack initiation. One side of each specimen was polished in the crack growth region with progressively finer emery paper to 600 grit. Cracks were monitored on this polished surface using a 33X traveling microscope with stroboscopic illumination. Crack length and num-

Table 2—Monotonic Tensile Properties

Property	4140 steel	weld deposit
Ultimate strength, S_u-MPa	577	772
0.2% Yield strength, S_y-MPa	338	598
True fracture stress σ_f-MPa	1049	1177
True fracture strain, ϵ_f	0.33	0.24
Reduction in area %	54	42

Table 3—Welding Conditions for Submerged Arc Welding

Heat input	30 KJ/cm
Preheating temperature	200°C
Current	500 A
Voltage	30 V
Welding speed	30 cm/min
Wire diameter	2.4 mm

Table 1—Chemical Composition (wt-%)

	C	Mn	P	S	Si	Ni	Cr	Mo	Ti	V	Cu
4140 steel	0.39	0.81	0.005	0.016	0.11	0.11	0.90	0.17	–	0.04	–
Electrode	0.07	1.57	0.008	0.006	0.38	1.65	0.02	0.35	<0.01	<0.01	0.096
Deposit	0.07	1.38	0.013	0.006	0.31	1.42	0.09	0.30	<0.01	<0.01	0.11

Fig. 2—Macroetch photograph of bead and plate weldment.

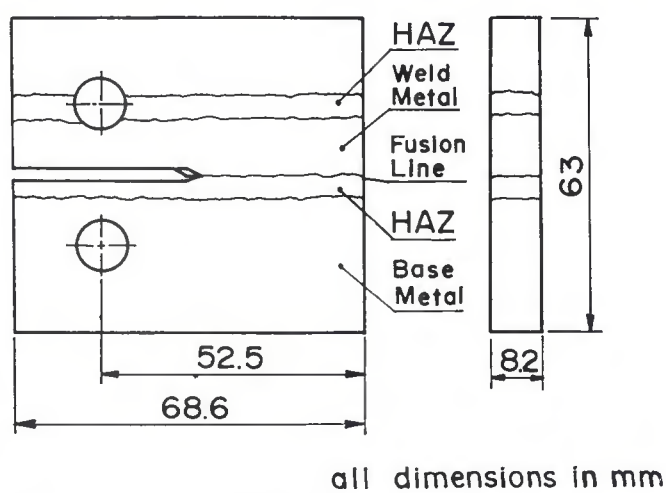

Fig. 3—Compact type, C(T) specimen.

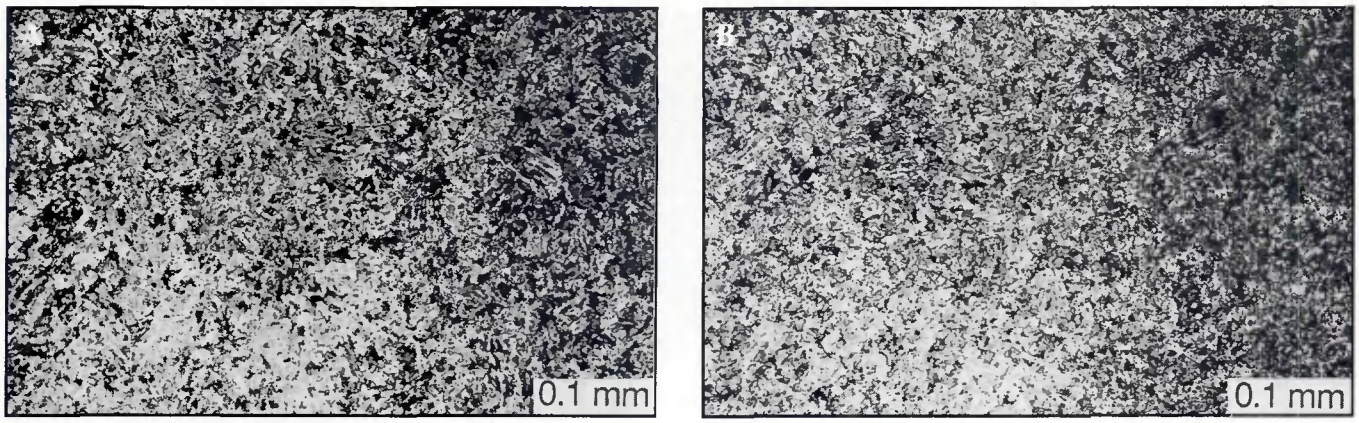

Fig. 4—Microstructure of base metal. A—As-received; B—after heat treatment.

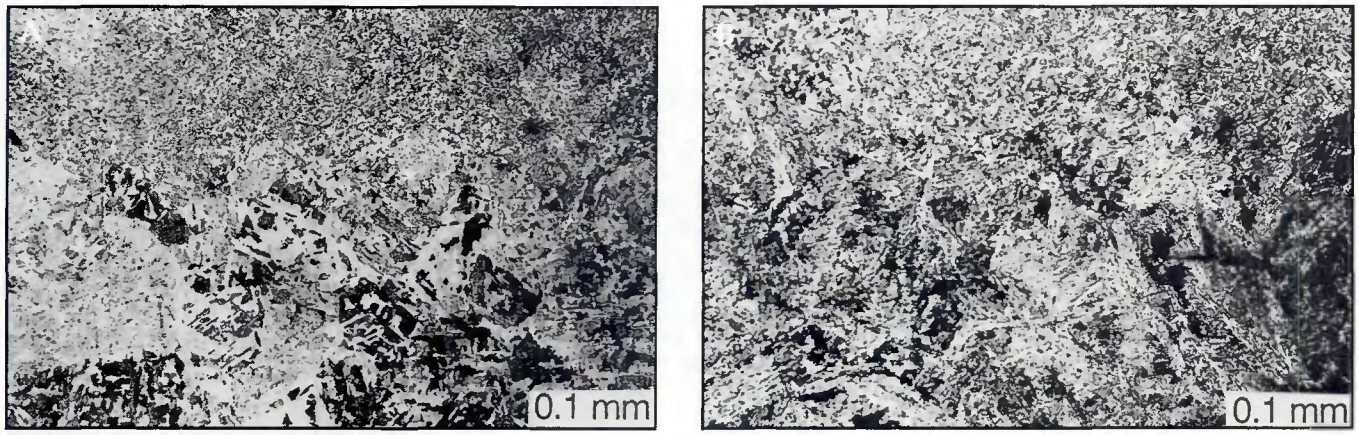

Fig. 5—Microstructure of weld HAZ material. A—As-welded; B—after PWHT.

ber of applied cycles were recorded every 0.25 to 1.0 mm (0.01 to 0.04 in.) of crack growth. Cracks were also occasionally monitored on the back side of the specimen to determine possible crack tip eccentricity during testing.

Constant-amplitude reference tests were obtained with two load ratios, $R = P_{min}/P_{max}$, of approximately zero and 0.5, using a positive haversine wave with a frequency of 15 to 25 Hz. The constant-amplitude data ranged from 10^{-8} to 10^{-6} m/cycle and hence were in Region II of the Paris log-log linear region. Single tensile overloads were applied at a crack length of 25 mm with an overload ratio of 2.5 as shown in Fig. 6. The overload ratio was defined as the overload force, P_{OL}, divided by P_{max} during the constant-amplitude portion of the test. Overloads were applied with a ramp wave at 0.125 Hz. All tests were terminated when the crack growth rate became too great to accurately measure crack length or when the uncracked ligament of the specimen (w-a) ceased to be predominately elastic. Both these criteria were essentially at about fracture.

All fatigue specimens were precracked approximately 2 mm (0.08 in.) to a total crack length, a, of 22 mm (0.87 in.). Precracking was usually done in three load-shedding steps as shown in Fig. 6. The reduction of P_{max} between load steps was less than 20% and the final precracking crack growth increment was greater than

$$\frac{3}{\pi}\left(\frac{K_{max}}{Sy}\right)^2 \qquad (1)$$

according to ASTM Standard E647. Final testing began at the conclusion of pre-

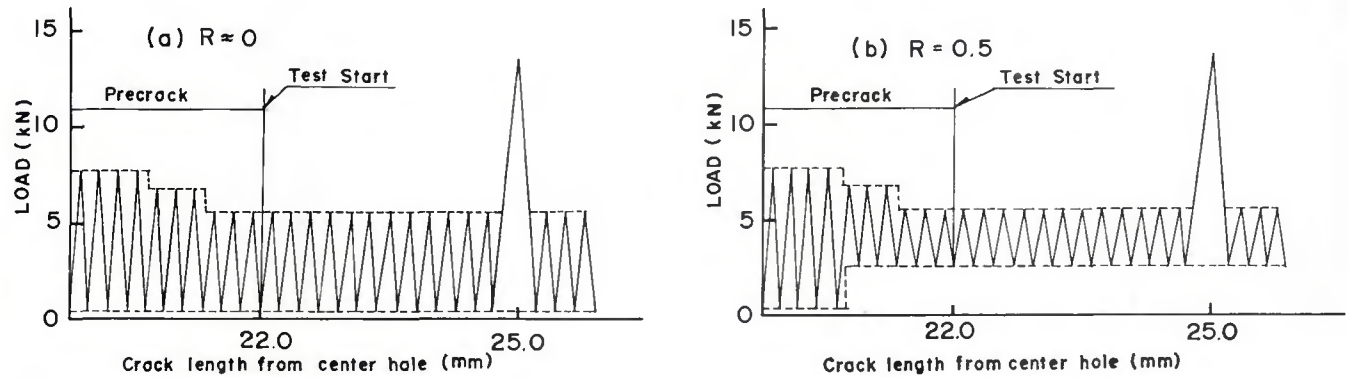

Fig. 6—Load spectrum for precracking, constant-amplitude and tensile overload.

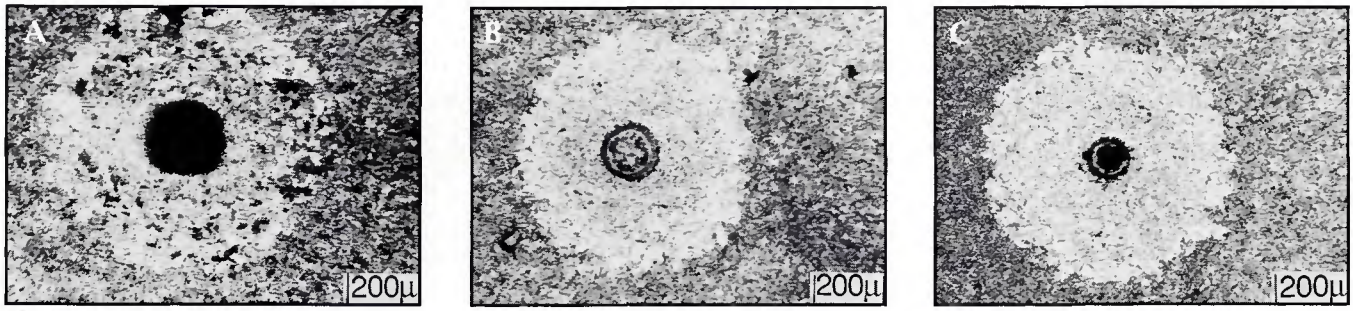

Fig. 7—Microstructure of recrystallization around indentation following annealing, base metal. A—740°C, 3 h; B—740°C, 7 h; C—740°C, 12 h.

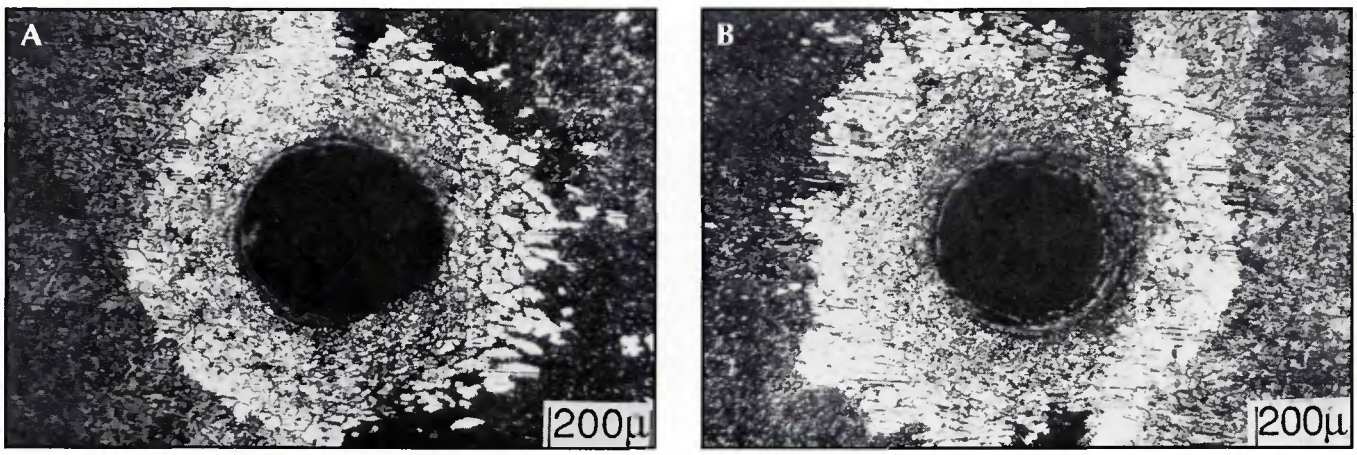

Fig. B—Microstructure of recrystallization around indentation following annealing, HAZ material. A—730°C, 7 h; B—730°C, 9 h.

cracking. All constant-amplitude fatigue tests had the final P_{max} equal to 5.34 kN and P_{min} equal to 0.13 kN for $R \approx 0$ tests, and P_{min} equal to 2.67 kN for $R = 0.5$ tests. The maximum stress intensity factor, K_{max}, just prior to overload was 23.5 MPa$\sqrt{m}$, and the overload stress intensity factor, K_{OL}, was 59 MPa$\sqrt{m}$.

Crack length, a, vs. applied cycles, N, data were reduced to da/dN vs. ΔK using a second-order incremental polynomial method for constant-amplitude tests and a secant method for single overload tests. The ΔK values were obtained from ASTM E647 as

$$\Delta K = \frac{\Delta P \ (2+\alpha)}{B\sqrt{W}(1-\alpha)^{\frac{3}{2}}}$$
$$(0.886 + 4.64\alpha - 13.32\alpha^2 + 14.72\alpha^3 - 5.6\alpha^4)$$

where $\Delta P = P_{max} - P_{min}$, $\alpha = a/W$, a = distance between crack tip and loading line, and B = thickness of specimen.

Recrystallization Technique for Fatigue Crack Plastic Zone Deformation

The plastic zone in the region of a growing fatigue crack is an important controlling feature of crack growth. Therefore, it is important when discussing fatigue crack growth to observe and quantify the deformation within the plastic region. Several methods exist for quantifying the plastic zone deformation at a crack tip. One method uses linear elastic fracture mechanics (LEFM), however, this fails when plastic zones become large. Crack tip opening displacement (CTOD) has been used to overcome the invalidity of LEFM under conditions of general plasticity. This method involves measurement of the crack tip deformation, but it is unable to reveal the plastic zone size ahead of the crack tip. To overcome these problems and to observe the crack region plastic zone directly, the recrystallization technique was adopted (Refs. 18–20). Specimens before and after overload were used with the recrystallization technique for both 4140 base metal and the welded HAZ. In order to obtain the proper recrystallization time, experiments were performed on the base metal and HAZ using the indentation technique. The results of these experiments performed in an argon atmosphere are shown in Figs. 7 and 8 following annealing and 5% Nital etchant usage. Here, the base metal was annealed at 740°C (1364°F) for 3, 9 or 12 h and the HAZ material was annealed at 730°C (1346°F) for 9 or 12 h. The lighter etched

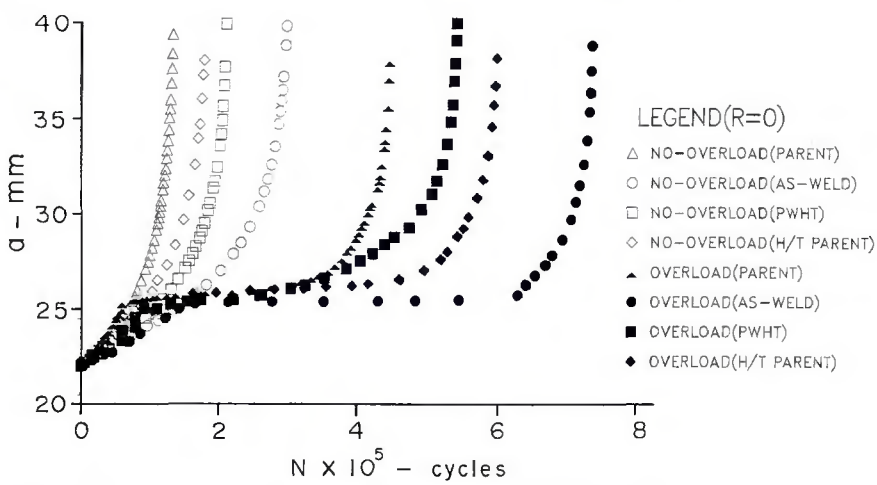

Fig. 9—Crack growth for no-overload and single overload conditions, $R \approx 0$.

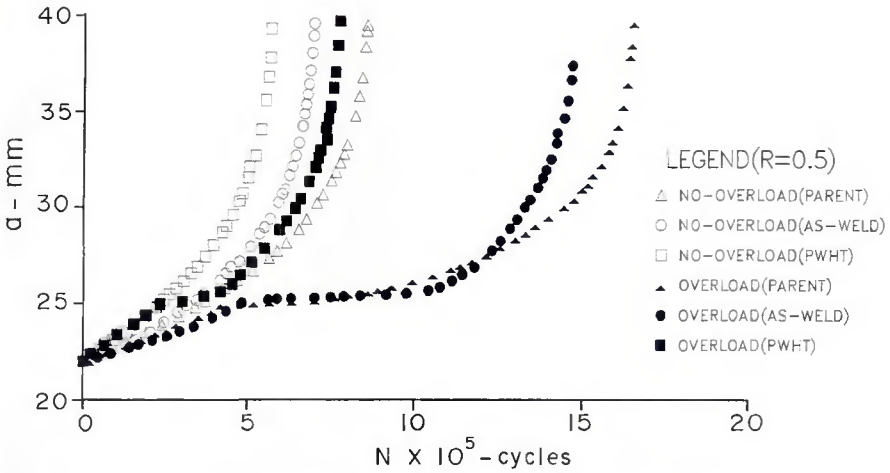

Fig. 10—Crack growth for no-overload and single overload conditions, R = 0.5.

regions around the indentations in Figs. 7 and 8 are the recrystallized zones. In both figures, the longer annealing times produced better results and these times were used with the C(T) specimens to find the fatigue crack recrystallization zones.

Test Results and Discussion

Fatigue Crack Growth Behavior

The constant-amplitude and single tensile overload crack length, a, vs. applied cycles, N, curves are given in Fig. 9 for all $R \approx 0$ tests, and in Fig. 10 for all R = 0.5 tests. Since each constant-amplitude test started at a = 22 mm with the same P_{max} for both R ratios, and each single tensile overload test had the same overload applied at a = 25 mm, followed by the same P_{max} value, these two figures provide substantial comparative results without reverting to da/dN vs. ΔK curves. In Figs. 9 and 10, the constant-amplitude data are represented by open data points and labeled no overload, and the overload data are represented by solid data points or crosses within the symbol. Also, for a given material condition, data points with the same shape are used for the constant-amplitude test and for the overload test. These selections make for easier comparison. The general schematic a vs. N curve for the no-overload curve and the overload curve is shown in Fig. 11. In addition, the retardation cycles, N_R, are defined in Fig. 11. The N_R is the horizontal displacement of the a vs. N curve following a single tensile overload.

From Figs. 9 and 10, the constant-amplitude fatigue crack growth curves were smooth and continuous and varied by a factor of only two or less at fracture for the given material conditions for each R ratio. This is a very small variation. The da/dN vs. ΔK curves for all constant-amplitude tests using the incremental second-order polynomial method are shown in Fig. 12. For a given R ratio, da/dN varies by a factor of two or less for the different material conditions. The biggest influence on constant-amplitude tests appears to be the R ratio and not the material behavior. The data are essentially log-log linear and hence satisfy the Region II Paris equation.

$$\frac{da}{dN} = A(\Delta K)^n \qquad (2)$$

From Figs. 9 and 10, the overload cycles

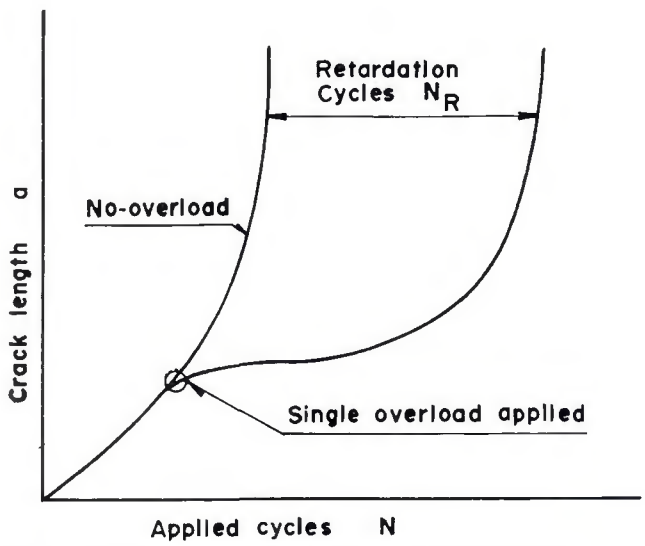

Fig. 11—Schematic diagram of fatigue crack growth retardation.

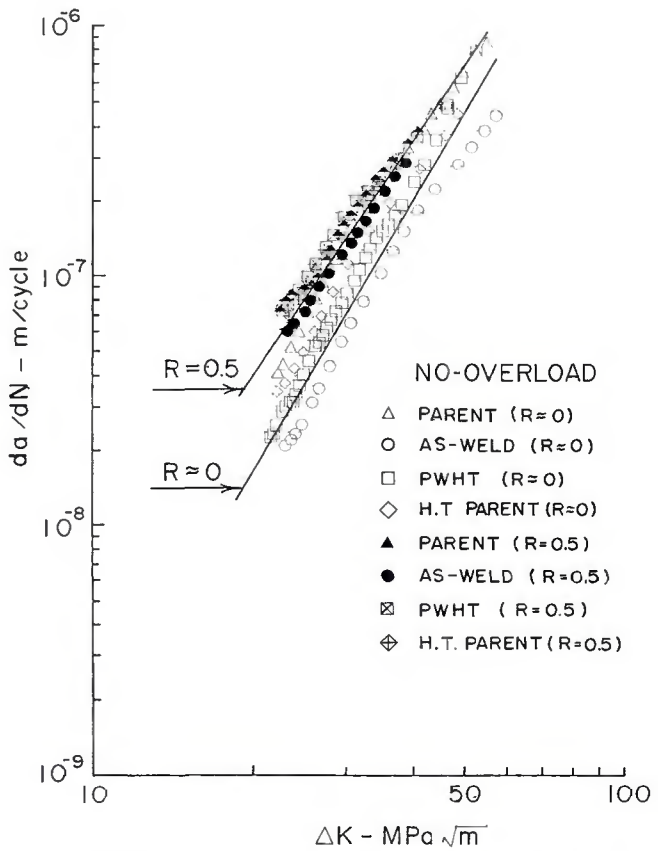

Fig. 12—Constant-amplitude (no overload) fatigue crack growth rate vs. ΔK.

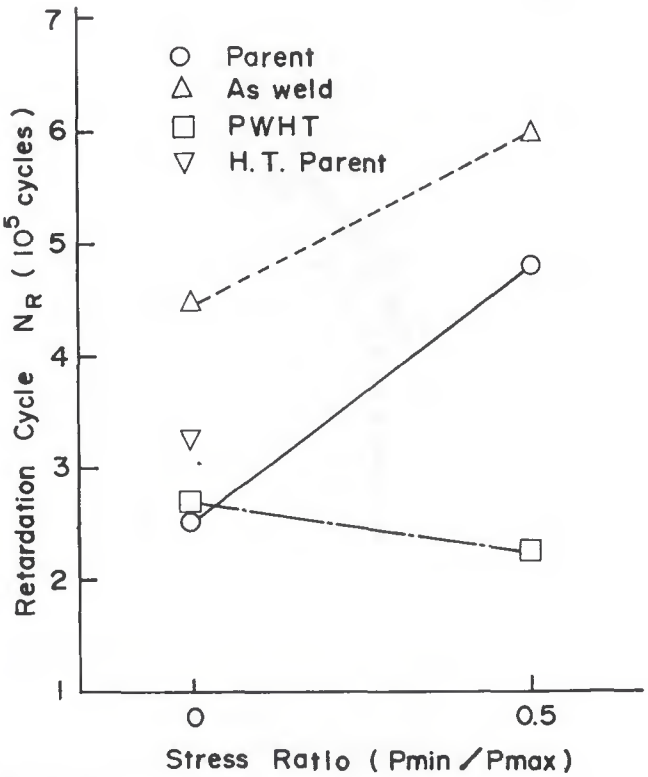

Fig. 13—Fatigue crack growth retardation, OLR = 2.5.

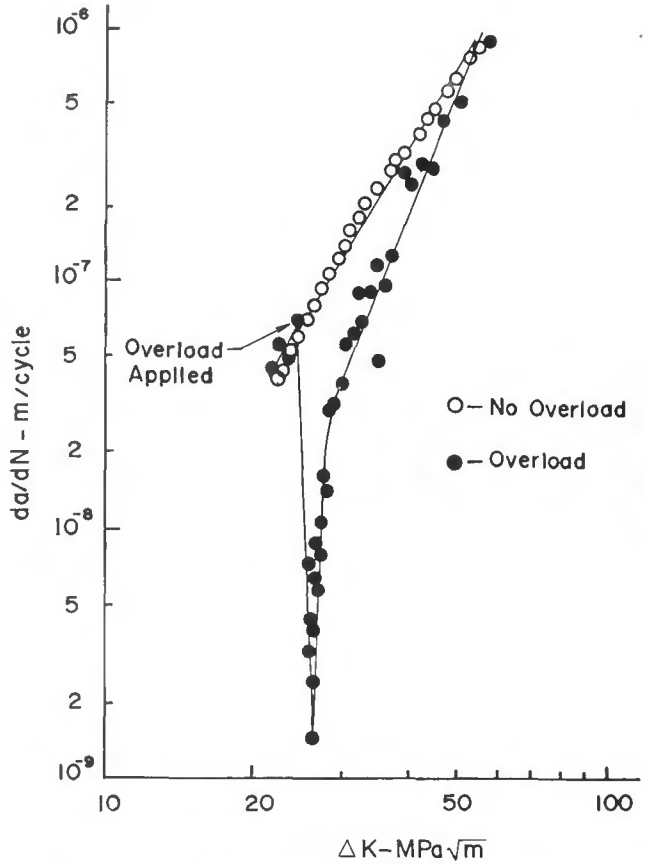

Fig. 14—Fatigue crack growth rate vs. ΔK for no-overload and single overload, parent metal, R ≈ 0.

to failure for a given R ratio fell within a factor of about 2.5 or less for all material test conditions. This again is a rather small variation between materials. The number of cycles of retardation, N_R, vs. R ratio is shown in Fig. 13 and varies from about 2×10^5 to 6×10^5 cycles. This represents fatigue crack growth life increases from about 400 to 600% for R ≈ 0, and 150 to 300% for R = 0.5. This indicates that all the material conditions investigated responded favorably to the single tensile overloads. In general, the R = 0.5 tests had a greater number of retardation cycles than R ≈ 0, however, the percent increase in fatigue life was better for the R ≈ 0 tests. The as-welded HAZ material with its higher strength had the greatest response to the single overloads compared to the other lower strength materials, as shown in Figs. 9, 10 and 13. This difference in retardation with strength for R ≈ 0 and 0.5 agrees with results by others (Refs. 21, 22). However, the differences in fatigue crack growth for the as-welded HAZ vs. the other materials must also incorporate residual stresses that have not been relaxed through PWHT. In fact, as-welded HAZ material and PWHT HAZ material have the same microstructure, but differ essentially in residual stress. Thus strength, R ratio and residual stresses are involved with the fatigue crack growth retardation.

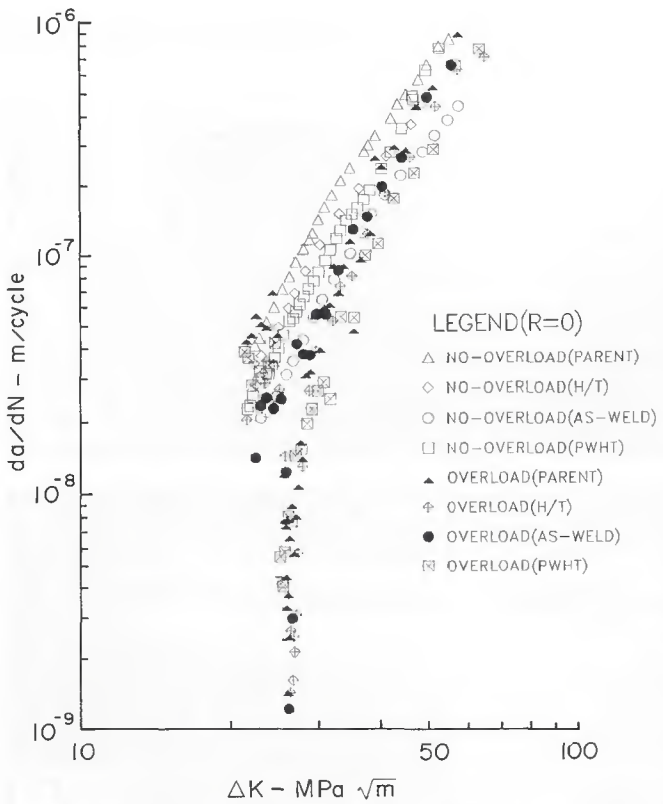

Fig. 15—Fatigue crack growth rate vs. ΔK, all materials, R ≈ 0.

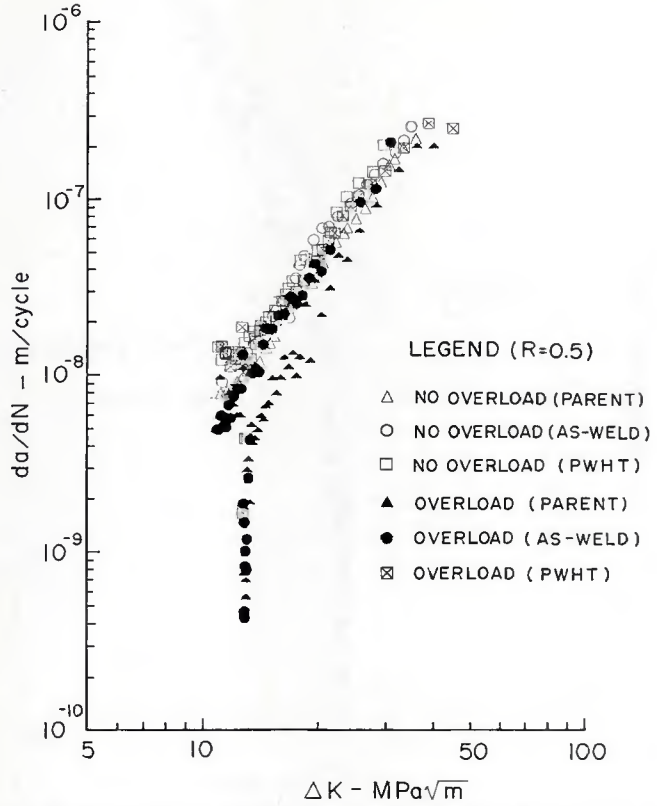

Fig. 16—Fatigue crack growth rate vs. ΔK, all materials, R = 0.5.

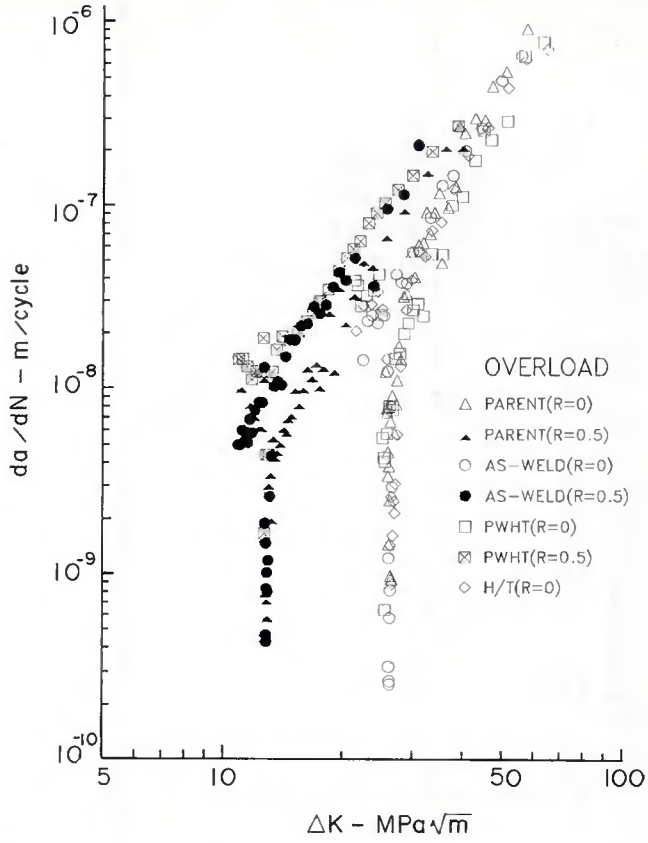

Fig. 17—Fatigue crack growth rate vs. ΔK for single overloads, all materials, R ≈ 0 and 0.5.

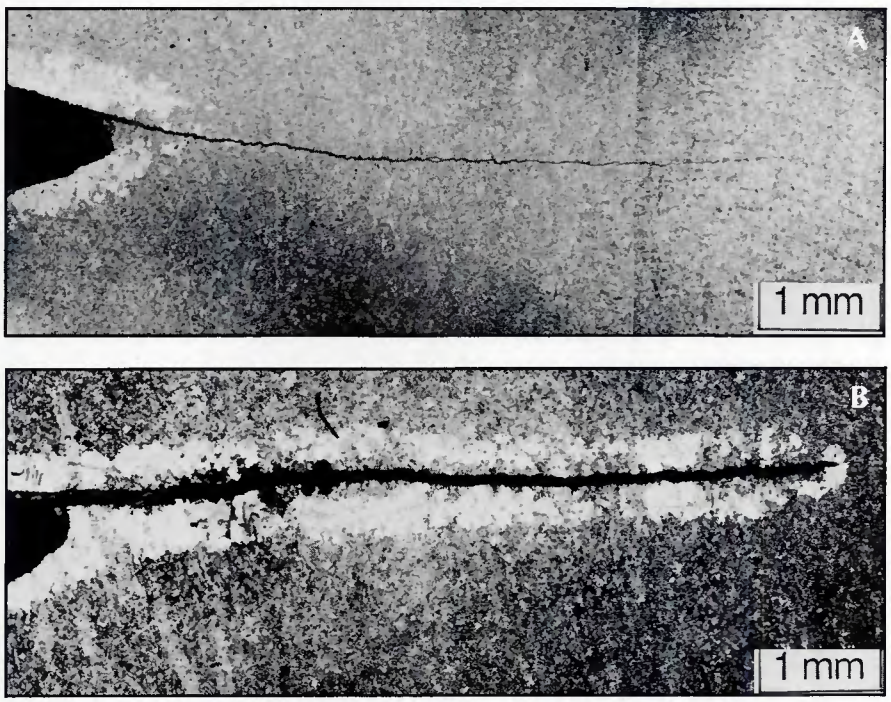

Fig. 18—Recrystallized zone around fatigue crack of base metal. A—No overload; B—single overload.

The a vs. N data for all tests were reduced to da/dN vs. ΔK. Typical results for the no-overload and overload conditions are shown in Fig. 14 for the base metal. Crack growth rates prior to the single tensile overload were above 10^{-8} m/cycle, while after the single overload, the rate dropped to almost 10^{-9} m/cycle. Convergence of the no-overload and overload data occurs as the crack grows out of the effective overload region. A superposition of no-overload and overload data similar to Fig. 14 is shown in Fig. 15 for all materials with R ≈ 0, and in Fig. 16 for all materials with R = 0.5. Open data points represent no-overload behavior. Greater scatter exists for the R ≈ 0 tests, however, all material tests again exhibit similar behavior.

Figure 17 shows the single overload data for both R ratios. It is quite evident here that the R ratio is the predominant factor when comparing da/dN with applied ΔK. Since crack closure was not monitored in these tests, an effective ΔK analysis cannot be made.

Recrystallization of Plastic Zones

Specimens of the base metal and the as-welded HAZ material were subjected to the recrystallization technique described earlier. Specimens with no overload and the single overload were evalu-

ated. Figure 18 shows the recrystallization regions for the base metal. There is no recrystallization zone around the fatigue crack for the no-overload condition, which means no strains occurred above the critical strain for showing recrystallization. The single overload base metal specimen shows some recrystallization region. Figure 19 shows the recrystallization zones around the fatigue crack for the as-welded HAZ. Larger plastic zones are shown for the as-welded HAZ, indicating more sensitivity with plastic deformation.

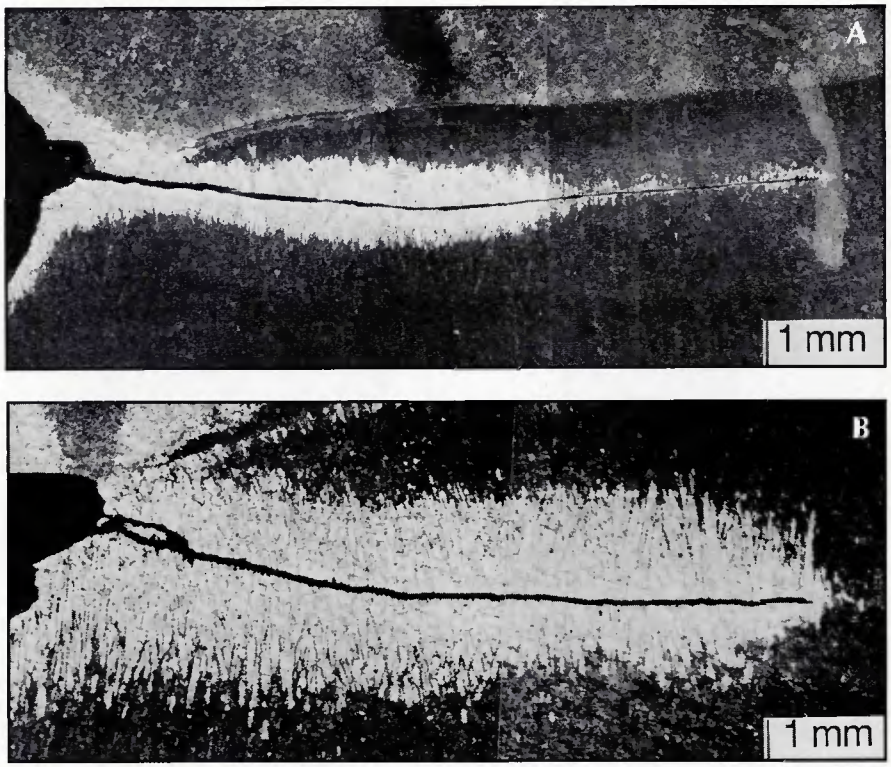

Fig. 19—Recrystallized zone around fatigue crack for as-welded HAZ. A—No overload; B—single overload.

Macrofractography

Typical macrofracture surfaces are shown in Fig. 20 for the constant-amplitude tests, and in Fig. 21 for the single overload tests. Three regions labeled A–C are shown in Fig. 20A. Label A indicates the precrack region and boundary. Label B denotes the fatigue crack growth test region, and label C represents the final ductile fracture region. In all cases, the fatigue cracks initiated at the chevron and grew toward the top of the fractographs. In all cases, the constant-amplitude fatigue crack growth regions are rather smooth, however, the R = 0.5 fracture surfaces were slightly smoother than for R ≈ 0. The single overload fracture surfaces indicate the overload marks are more intense for R ≈ 0 than for R = 0.5. The overload crack tip curvature is somewhat eccentric; however, the curvature still satisfied ASTM E647 requirements. Overload markings indicate a small difference in the 25-mm crack length at overload existed. This was not a significant factor, however.

Scanning Electron Microscopy

Typical SEM fractographs for the constant-amplitude tests with base metal, as-welded HAZ and PWHT conditions are shown in Fig. 22. Two magnifications are shown for each material condition. Direction of fatigue crack growth is from bottom to top in all fractographs. Very few distinct striations were evident on any of the surfaces; yet, so-called ductile quasi-striation crack growth morphology existed. All materials showed porosity, inclusions and secondary cracking, and appeared rather similar except as-welded and PWHT material had more debris, more microcracks and greater roughness.

Figure 23 shows the effect of the single tensile overload for the base metal, as-welded HAZ and PWHT material conditions. Again, two magnifications were used for each material condition. The up-

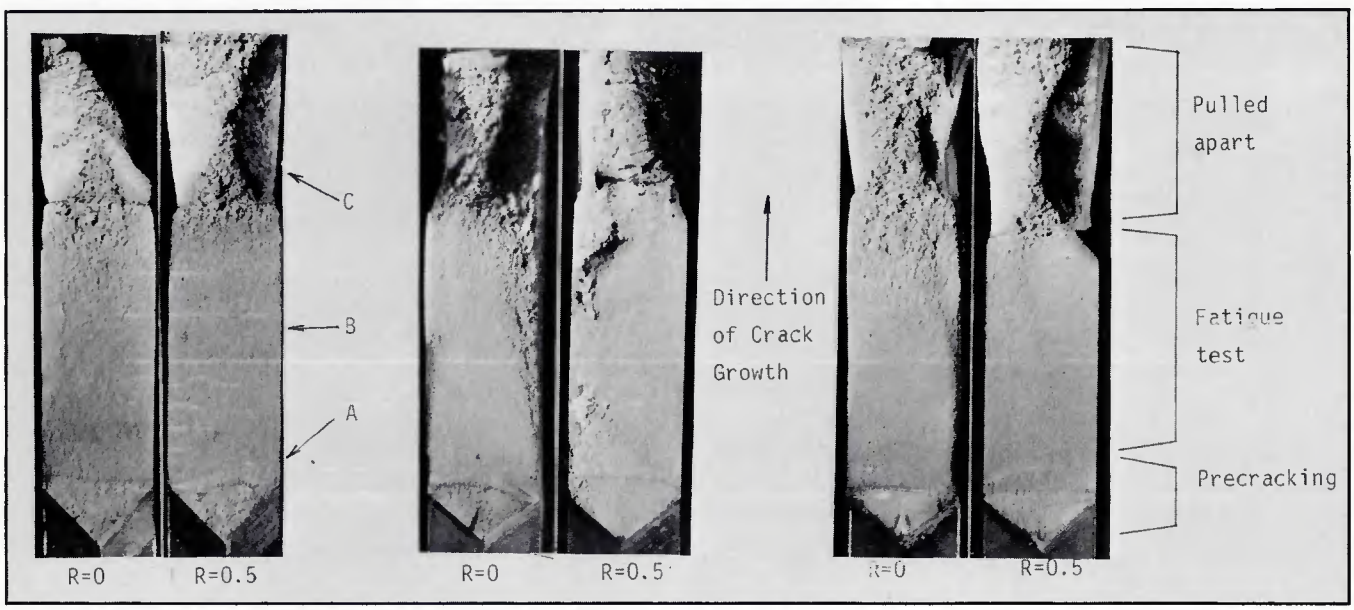

Fig. 20—Typical macro fracture surfaces for constant amplitude tests.

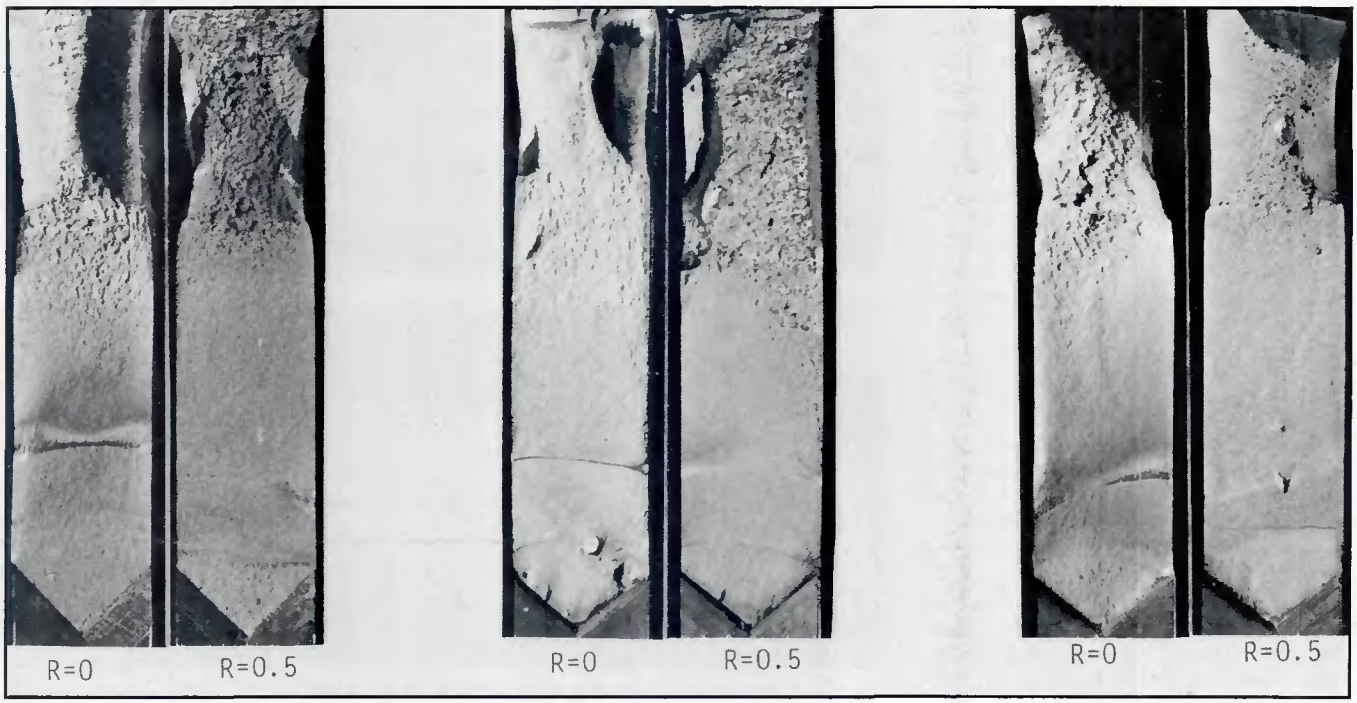

Fig. 21—Typical macro fracture surfaces for single overload tests.

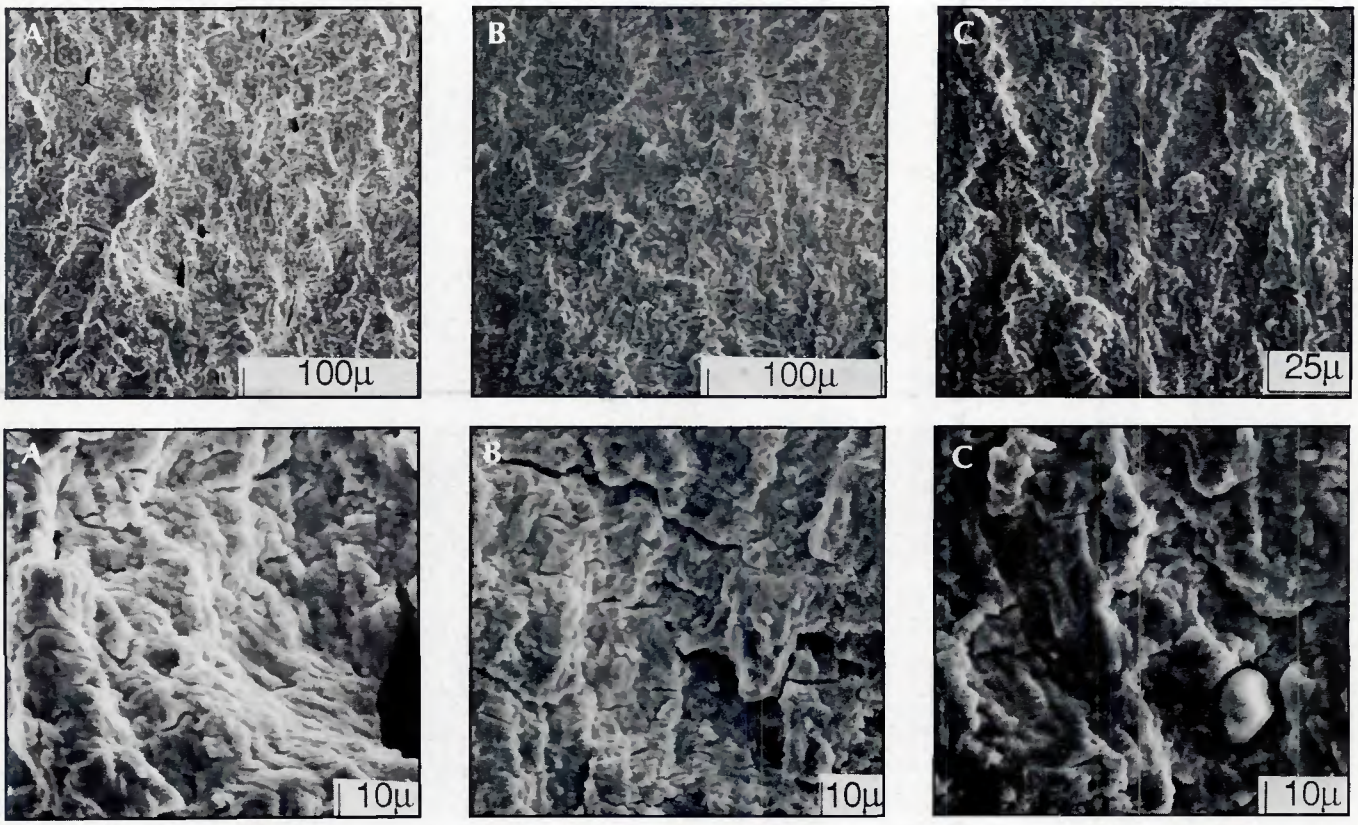

Fig. 22—Typical SEM fractographs, no overload. A—Base metal; B—as-welded HAZ; C—PWHT HAZ.

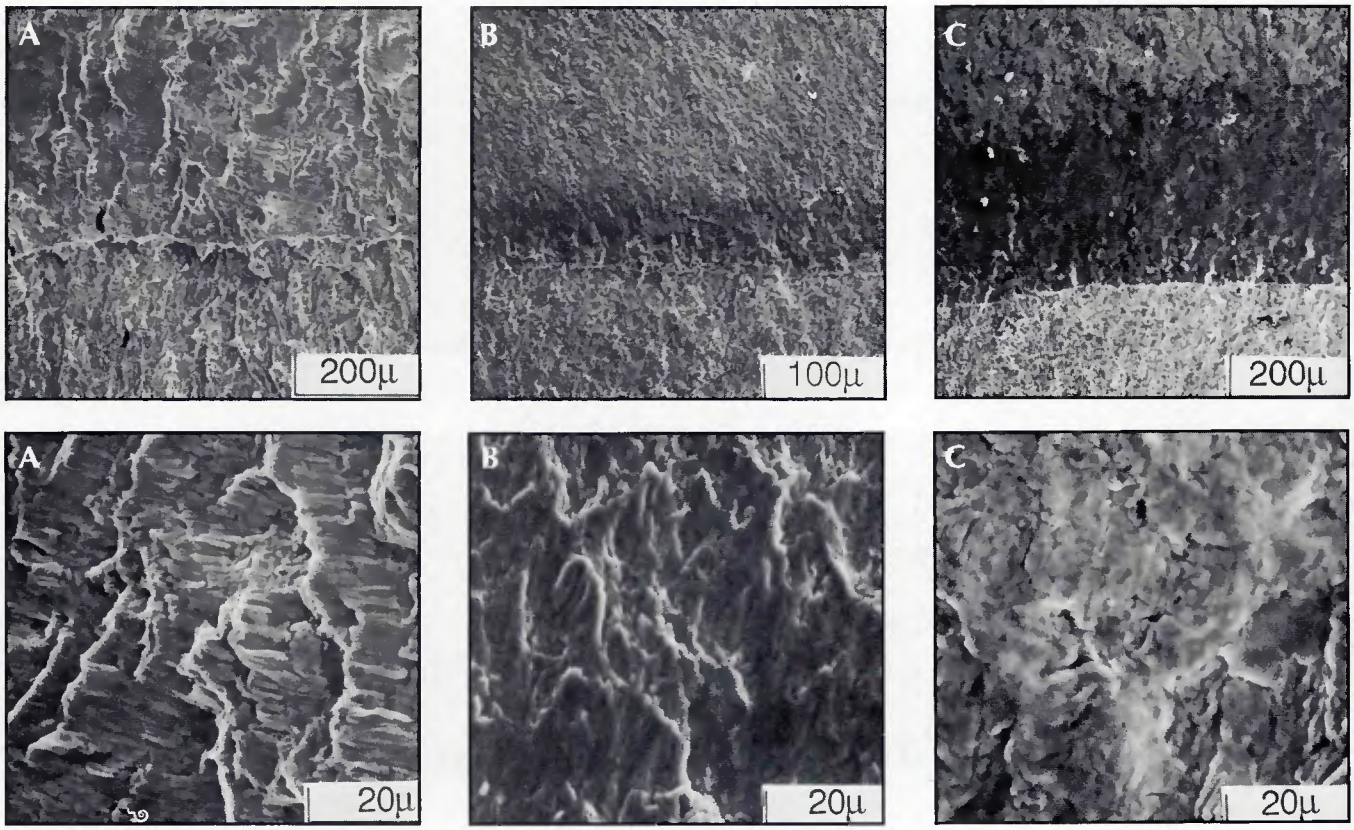

Fig. 23 — Typical SEM fractographs after single overload. A — Base metal; B — as-welded HAZ; C — PWHT HAZ.

per fractographs, taken at 100X or 200X magnification, show the tensile overload markings. The lower fractographs show fracture surface at 1000X magnification after the overload was applied. Substantial crack closure following the overload often tended to obscure some of the fatigue crack growth markings. In general, no great differences in the fatigue crack growth morphology existed between the different material conditions tested. This is consistent with the lack of substantial differences between material conditions.

Summary and Conclusions

The following information is based upon room-temperature fatigue crack growth, recrystallization and SEM investigations of the 4140 base metal, heat treated base metal (PWHT), and as-welded HAZ material using automatic submerged arc welding with the PWHT HAZ material subjected to constant-amplitude loading (no-overload) and single tensile overloads using an OLR of 2.5.

1) All four conditions had essentially the same constant-amplitude fatigue crack growth resistance in the Paris log-log linear region. Differences in fatigue life and fatigue crack growth rates were within a factor or two. The stress ratio, R, had the greatest influence on constant-amplitude fatigue crack growth rates as a function of ΔK. R = 0.5 had higher rates than $R \approx 0$ by a factor of 2 to 5.

2) All four material conditions responded favorably to the single tensile overloads. The differences between material response for these single overloads were small, within a factor of 2.5. Retardation of fatigue crack growth varied from 2×10^5 to 6×10^5 cycles for the four material conditions, which represented an increase in fatigue crack growth life from 150 to 600%. The greatest retardation response occurred in the as-welded HAZ material under both $R \approx 0$ and 0.5 test conditions.

3) The recrystallization technique for determining plastic zones before and after single overloads was only partially successful. The as-welded HAZ material was more sensitive than the base metal to the recrystallization technique.

4) Scanning electron microscope results indicated many similarities in fatigue crack growth morphology for the four material systems. Ductile quasistriations, porosity, inclusions and secondary cracking were evident with all four material conditions. The principal differences were the greater amounts of debris, microcracks and roughness in the as-welded and PWHT HAZ materials.

References

1. H. I. McHenry and J. M. Potter, editors, *Fatigue and Fracture Testing of Weldments*, ASTM STP, to be published.

2. Dolby, R. E. 1972. Welding and fracture initiation in QT low-alloy steels. *Metallurgy*, p. 159.

3. Rolfe, S. T., and Barsom, J. M. 1977. *Fracture and Fatigue Control in Structures*, Prentice-Hall.

4. Burdekin, F. M. 1967. Initiation of brittle fracture in structural steels. *British Welding Journal*, Vol. 12, p. 649.

5. Phillip, R. H. 1983. In situ determination of transformation temperature in the weld heat-affected zone. *Welding Journal* 62(1): 12-s to 18-s.

6. Frost, R. H., Edwards, G. R., and Rheinlander, A. D. 1981. A constitutive equation for the critical energy input during electroslag welding. *Welding Journal* 60(1): 1-s to 6-s.

7. Kameda, J., Takahashi H., and Suzuki, M. 1976. Residual stress relief and local embrittlement of weld HAZ in reaction pressure vessel steel. *IIW Doc. No. X-800-76* and *Doc. No. IX-1002-76.*

8. Dolby, R. E. 1972. Fracture toughness comparison of weld HAZ and thermally simulated microstructures. *British Welding Journal* p. 59.

9. Dawes, M. G. 1976. Weld metal fracture toughness. *Welding Journal* 55(12):1052-1057.

10. Suzuki, M., Takahashi, H., and Kameda, J. 1976. Postweld heat treatment and embrittlement of weld HAZ in a low-alloy steel. *Welding Journal of JWS*, Vol. 45, No. 1, p. 6.

11. Bloom, J. M. 1981. An analytical assessment of the effect of residual stress and fracture properties on service performance of various weld repair processes. *Journal of Pressure Vessel Technology*, ASME, Vol. 103, p. 373.

12. Joshi, A., and Stein, D. F. 1972. *Temper Embrittlement of Low-Alloy Steels*. ASTM STP

499, p. 59.

13. Hippsley, C. A., Knott, J. F., and Edwards, B. C. 1980. A study of stress relief cracking in 2¼ Cr-1 Mo steel. *Acta Metallurgica,* Vol. 28, p. 869.

14. Lim, J. K., and Chung, S. H. Stress effect on PWHT embrittlement *Fatigue and Fracture Testing of Weldments,* Edited by H.I. McHenry and J.M. Potter, ASTM STP. To be published.

15. *Fatigue Crack Growth under Spectrum Loads,* 1976. ASTM STP, p. 596.

16. ASTM Standard E647-83. 1983. Standard test method for constant load amplitude fatigue crack growth rates above 10 m/cycle. *1984 Annual Book of ASTM Standards,* Vol. 03.01, p. 711.

17. Dolby, R. E. 1971. Welding and fracture initiation in QT low-alloy steels. *Metal Construction and British Welding Journal,* Vol. 4, p. 99.

18. Iino, Y. 1975. Cyclic crack tip deformation and its relation to fatigue crack growth. *Engineering Fracture Mechanics,* Vol. 7, p. 205.

19. Iino, Y. 1976. Accumulated plastic zone around fatigue crack in Type 304 stainless steel. *Metal Science,* Vol. 10, p. 159.

20. Shoji, T. 1976. Crack-tip blunting and crack opening displacement under large-scale yielding. *Metal Science,* Vol. 10, p. 165.

21. Njus, G. O., and Stephens, R. I. 1977. The influence of yield strength and negative stress ratio on fatigue crack growth delay in 4140 steel. *International Journal of Fracture,* Vol. 13, No. 4, p. 455.

22. Petrak, G. J., and Gallagher, J. P. 1975. Predictions of the effect of yield strength on fatigue crack growth retardation in HP-9Ni-4 Co-30 C steel. *Journal of Engineering Materials and Technology* p. 206.

WRC Bulletin 343
May 1989

Destructive Examination of PVRC Weld Specimens 202, 203 and 251J

This Bulletin contains three reports:

(1) Destructive Examination of PVRC Specimen 202 Weld Flaws by JPVRC
By Y. Saiga

(2) Destructive Examination of PVRC Nozzle Weld Specimen 203 Weld Flaws by JPVRC
By Y. Saiga

(3) Destructive Examination of PVRC Specimen 251J Weld Flaws
By S. Yukawa

The sectioning and examination of Specimens 202 and 203 were sponsored by the Nondestructive Examination Committee of the Japan Pressure Vessel Research Council. The destructive examination of Specimen 251J was performed at the General Electric Company in Schenectady, N.Y., under the sponsorship of the Subcommittee on Nondestructive Examination of Pressure Components of the Pressure Vessel Research Committee of the Welding Research Council. The price of WRC Bulletin 343 is $24.00 per copy, plus $5.00 for U.S., or $8.00 for overseas, postage and handling. Orders should be sent with payment to the Welding Research Council, Room 1301, 345 E. 47th St., New York, NY 10017.

WRC Bulletin 344
June 1989

This Bulletin contains two reports covering three-dimensional finite element analysis of 45-deg lateral branch pipe models.

(1) Three-Dimensional Finite Element Analysis of PVRC 45-Degree Lateral Model 4 (d/D = 0.5, D/T = 40) under Out-of-Plane Moment Loading on Branch Pipes
By P. P. Raju

(2) Three-Dimensional Finite Element Analysis of 45-Degree Lateral Model 2 (d/D = 0.5, D/T = 10) under Out-of-Plane Moment Loading on the Branch Pipe
By P. P. Raju

Publication of these reports was sponsored by the Joint Task Group on Laterals of the Subcommittee on Piping, Pumps and Valves, and the Subcommittee on Reinforced Openings of the Pressure Vessel Research Committee of the Welding Research Council. The price of WRC Bulletin 344 is $16.00 per copy, plus $5.00 for U.S., or $8.00 for overseas, postage and handling. Orders should be sent with payment to the Welding Research Council, 345 E. 47th St., Room 1301, New York, NY 10017.